Unbiased Wide Range Survey for RR Lyraes

Daichi Hiramatsu[1, *] and Corey Mutnik[1, †]

[1] *Department of Physics & Astronomy, University of Hawai'i at Mānoa 2505 Correa Rd, Honolulu, HI, 96822, USA*

By Thursday (4/18) we need: well thought out section titles and plots that show all the points we wanna make

remake prob(f) plot with all 300,000 stars (not only 80,000)

LS analysis on ATLAS Pathfinder Telescope data, verified PS variability criteria

1. INTRODUCTION

Initially, determination of variability was going to be achieved using data collected by the *gri Project*[1]. In order to reduce aliasing, extra observations needed to be collected. Desired galactic coordinates had to be converted to right ascension (RA) and declination (Dec), before feeding observations to the Pathfinder telescope. Observation procedures are discussed in § 2 2.2. Our field of view (FOV) spanned approximately 340 deg^2 and contained 1.5 billion stars. Once we received the reduced image data from the ATLAS pipeline[1], the 315, 992 most variable candidates were isolated and subjected to more comprehensive variability classification. Methods used to identify RR Lyrae stars are discussed in § 5.

Verification of RR Lyrae candidates also allowed for comparison to external variable catalogs. Completeness and evaluation of multiple RR Lyrae catalogs is discussed in § 7. Various models of RR Lyrae distributions exist, with little to no verification. In order to validate and refine such models, classification of stars is required. Such classifications are made possible by collecting observations and performing rigorous analysis.

2. ATLAS PATHFINDER OBSERVATIONS

We used the 0.18 m Asteroid Terrestrial-impact Last Alert System (ATLAS) Pathfinder telescope[2] at the Mauna Loa. The FOV of this telescope is 5.2°, with the angular resolution (effective PSF FWHM) of 5". Thanks to its wide FOV, it is suitable for our project, wide field study. The spatial resolution, however, is not great. For this reason, we chose our field to be slightly off the galactic plane. To estimate dust reddening and to determine periods of RR Lyrae stars accurately, we used the all three of g, r, and i filters.

2.1. SNR Calculation

To calculate an appropriate sampling frequency and SNR, typical RR Lyrae light curves[3] were used with artificially introduced gaps and noise following the Gaussian distribution. To determine distances from the PL relations[4] within $\simeq 5\%$ accuracy assuming typical metalicity $Z = 0.001$, we need periods within $\simeq 1\%$ accuracy. The period range of RR Lyrae stars is 0.05 to 1.2 days [5] which contrains the sampling frequency. By using the Lomb-Scargle analysis (discussed in § 4), it was found that 15 nights with 10 observations/night is the lower limit sampling duration and rate to achieve the desired period accuracy. Since the magnitude fluctuations of RR Lyrae are typically in the range of 0.3 to 2.0 mags [6], the uncertainty in magnitude was taken to be 0.1 mags, and the changes, 0.01 to 0.1 mags, in the uncertainty did not affect the period determinations significantly. Thus we only needed 10% photometry. For $m_g = m_r = 16$ and $m_i = 15.7$, an exposure time of 20 sec yields 10% photometry for the ATLAS pathfinder telescope[2].

2.2. Data Collection

Using the Pathfinder telescope, observations were made at two galactic latitudes ($b = \pm 5°$) and spanned a range of galactic longitudes ($202° \leq l \leq 232°$). Observations discussed here indicated the center of each FOV. Exposures were collected for 20 sec and separated by 3° longitudinally. For implementation by the Pathfinder telescope, a conversion to RA and Dec was made; giving a range of roughly $90 \leq RA \leq 120°$ and $-23° \leq Dec \leq 18°$, as shown by Figure 8. In total, our observation encompassed roughly 340 deg^2. To account for the 0.05 ° gap between the detectors, a 0.1 ° offset in RA was implemented on every other night. Spanning 20 nights (including 5 additional nights to the lower limit sampling duration of 15 nights), 10 observations a night were collected on 3/8/16-3/27/16. Luckily, all of these nights had

weather perfectly attuned for observations. Half a night of observations were lost on 3/19/26, due to a crash of the server controlling the telescope.

Observations were traced out by moving the FOV by 3° longitudinally, starting at $b = -5°$, $l = 202°$ and ending at $b = -5°$, $l = 232°$. Once observations at $b = -5°$ were complete, the FOV was shifted to $b = +5°$, $l = 232°$. Then observations were collected in steps of 3°, longitudinally, until $l = 202°$.

2.3. Object Cuts

Any stellar magnitudes that returned with zero error, after being reduced by the ATLAS pipeline[1], we not used in variability determination. In order for an identified star to be considered for variability testing, we required a minimum of 12 "good" observations. A "good" detection is meets the minimum PSF, does not fall on the edge of each 1 deg^2 FOV, and was observed with clear skies. A minimum of 12 observations was deemed necessary, in order to eliminate aliasing, as discussed in § 4. After observation cuts were applied, 1.5 Billion stars remained in our FOV.

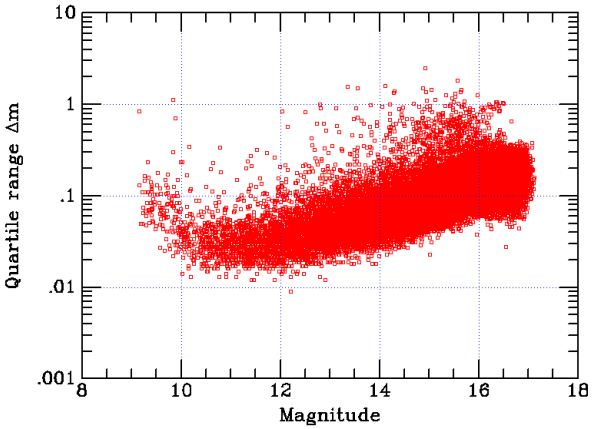

FIG. 1: *Lower quartile variance as a function of* m_r.

In order to exploit the lower quartile variance, shown in Figure 1, a factor of $0.2m$ was added to account for Poisson error. The higher a star deviates from the average value, the more likely it is variable. This flagged 315,992, of the observed 1.5 billion, for further variability verification.

As a result of running FLS, the most variable candidates fell below $logPr(rnd) \leq -45$, shown in Figure 3. An in depth discussion how $logPr(rnd)$ works can be found in *Numerical Recipes*[7,8]. Using $logPr(rnd)$ made it impossible to miss any variable star with $0.05 \leq Period \leq 1.2$ [6]. It is statistically improbable that any observed variable star wasn't flagged. If any variable stars were not identified, they must have lower period variations and are therefore not classified as RR Lyrae.

3. CONSTRUCTING STELLAR LIGHT CURVES

Once observations were made, the data had to be sorted and grouped. Resolving individual stars encompassed matching the coordinates of each object with all other collected data, to within a tolerance of 0.001°. The particular sorting algorithm, written by J. Tonry[1], is discussed in § 7 7.3. Grouping data with such high precision eliminates the possibility that observations of a particular object overlap. In doing so, we remove contamination and make each grouping as characteristic as possible, for its intended star. Figure 2 shows an example light curve, constructed by grouping all observations of a single star. Apparent magnitude is plotted against time, with m_g, m_r, and m_i plotted in green, red, and blue, respectively.

4. PERIODOGRAM ANALYSIS

To extract periods from light curves, the Fast Fourier Transform (FFT) is usually used. For our data, however, FFT is not optimal due to the data gaps. To deal with the data gaps, the Fast Lomb-Scargle (FLS) periodogram analysis[8,9] was used in this study because of its high computational efficiency. FLS extracts not only periods but also the significance levels of periods in the form of $\log Pr(rnd)$. The more negative the significance levels are, the more significant the periods are, so we can used the significance levels to statistically select periodic-variable candidates. The outputs, $\log Pr(rnd)$ and frequency, of FLS is shown in Figure 3. Since our observational period is roughly a day, there are major aliasings at the periods with integer multiple of a day. To avoid the aliasing and statistically select candidates, we masked a period range with high significance level (≤ -12.5) and used the masked range for the further analyses.

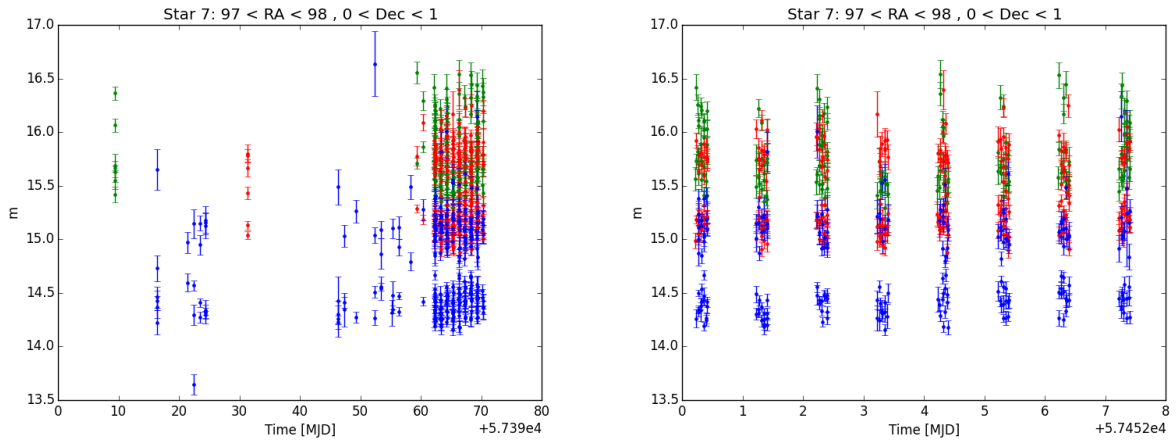

(a) (b)

FIG. 2: *Light Curve of a variable star. Panel '(a)' shows a light curve constructed using all collected and ATLAS data. Panel '(b)' is a restricted selection of '(a)', not showing any observations made by ATLAS.*

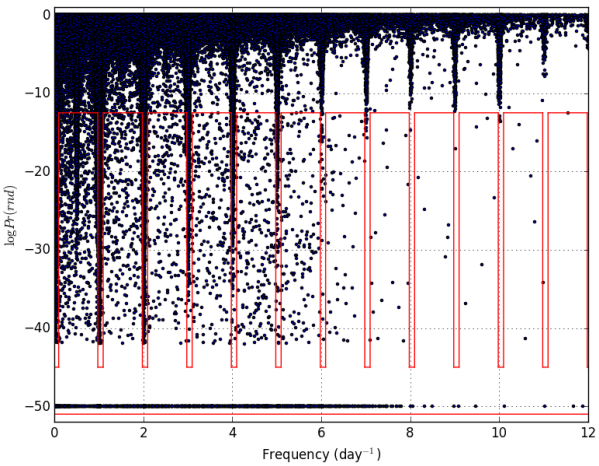

FIG. 3: $\log Pr(rnd)$ *vs frequency* (day^{-1}) *of* $315,992$ *stars selected by the quartile criteria. The region enclosed by the red lines define the masked regions with high significance level (*$\log Pr(rnd) < -12.5$*) and no aliasing (*$0.02 <$ *frequency* < 0.98*,* $1.02 <$ *frequency* < 1.98*, etc.). The masked region contains* $5,658$ *stars.*

5. RR LYRAE SELECTION CRITERIA

To identify RR Lyrae stars, we applied three criteria: period consistency among gri filters, Fourier Sine Series χ^2/ndf, and Fourier Sine Series amplitude.

5.1. Period Consistency Among gri filters

The first criterion was the consistency of periods calculated by FLS from g, r, and i filters individually since RR Lyrae stars should have identically the same period in each filter in the range of 0.05 to 1.2 days [5]. We checked whether each filter period agreed within 0.04 days $\simeq$ 1 hour with each other.

5.2. Fourier Sine Series χ^2/ndf

The second criterion was χ^2/ndf calculated using the Fourier Sine Series (FSS). Since the RR Lyrae light curves are more or less sinusoidal, FSS with a few terms should be able to represent the light curves for certain accuracy. We used FSS in the form;

$$\text{FSS} = \sum_{n=1}^{N} \sin\left(\frac{n\pi t}{P} + \phi_n\right) \qquad (1)$$

where P is the calculated period from FLS, ϕ_n is the phase, and N of up to 6 (for larger N, the computations were unstable; huge errors in the parameter estimations). We required the χ^2/ndf be within sigma deviation of 3, so $\chi^2/\text{ndf} \sim \sigma^2 < 9$.

5.3. Fourier Sine Series amplitude

The third criterion was the amplitude of FSS. As mentioned before, the amplitude range of RR Lyrae stars is 0.3 to 2.0 mags, so we set the amplitude ranges of FSS to be 0.15 to 2.15 mags by taking 10% photometry into account (1.5σ limit). The four major types of RR Lyrae found by using out criteria are show in Figure 4. The three criteria yielded $1,239$ RR Lyrae stars out of $5,658$ candidates in the masked region.

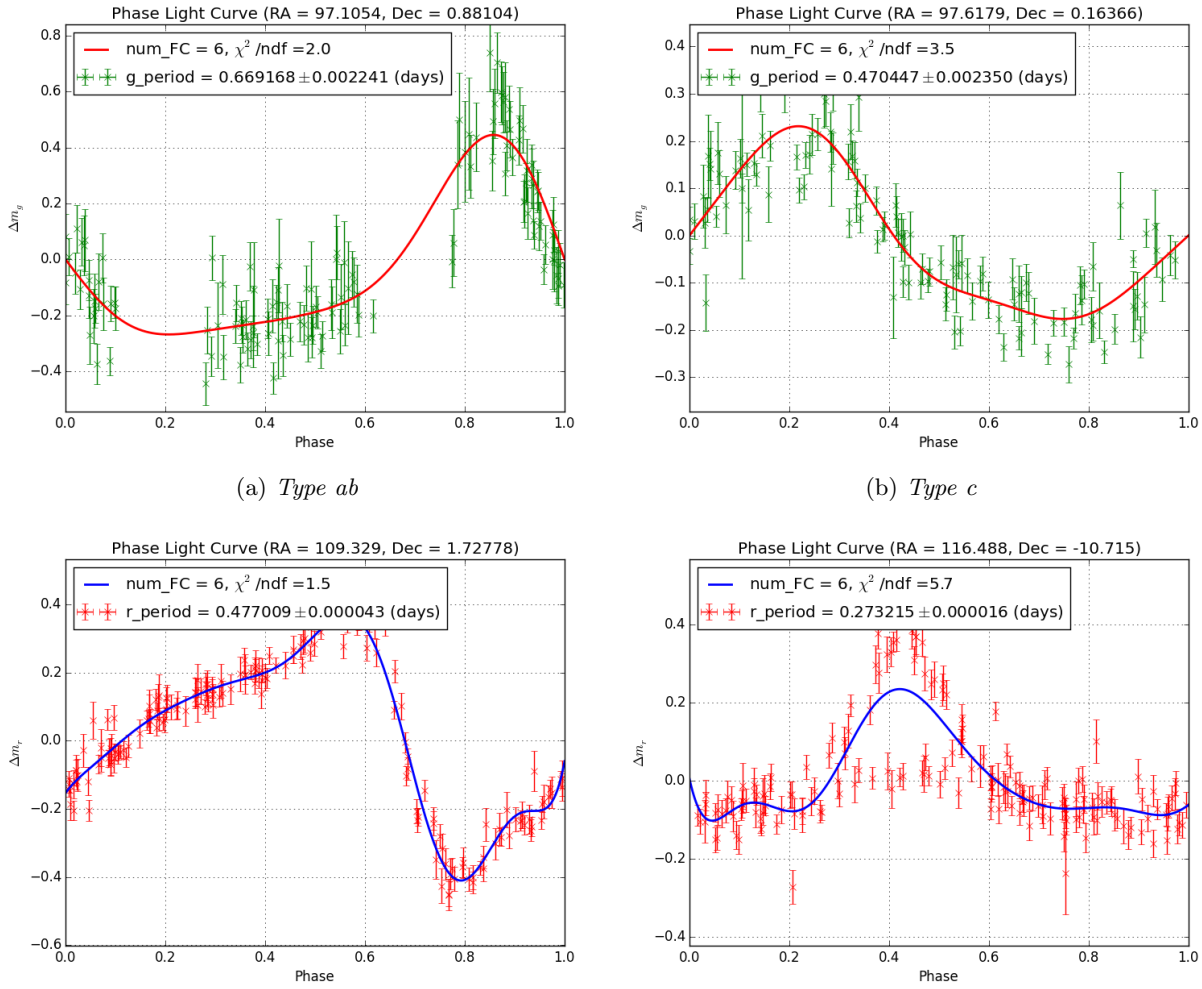

(a) *Type ab*

(b) *Type c*

(c) *Blazhko Modulated*[3]

(d) *Period Doubling*

FIG. 4: *Four major types of RR Lyrae phase light curves.*

5.4. Period Error Estimation

Assuming the Gaussian statistics and Taylor expanding χ^2 with respect to angular frequency, the estimated error model for angular frequency, $\delta\omega$, was constructed[1] and expressed as;

$$1 = \frac{\chi^2(\omega)}{\mathrm{ndf}} - \frac{\chi^2(\omega_0)}{\mathrm{ndf}} \simeq \frac{A^2}{2}\delta\omega^2 \sum_{i=1}^{\mathrm{ndp}} \frac{(t_i - \bar{t})^2}{\delta m_i^2} \qquad (2)$$

where ω_0 is the calculated angular frequency by FLS, A is the calculated amplitude by FSS, ndp is the number of data points, $\bar{t}$ is our mean observation Julian Date, and δm is the uncertainty in magnitude. The choice of time origin was tricky since the model allows arbitrary time origin, so we used $\bar{t}$ as a reasonable choice. Then the period uncertainties were estimated as;

$$\delta P = \frac{d}{d\omega}\left(\frac{2\pi}{\omega}\right) = \frac{2\pi}{\omega^2}\delta\omega\,. \qquad (3)$$

The mean period uncertainty of $1,239$ RR Lyrae stars was calculated to be $\simeq 0.15\%$, which shows the our SNR calculations for period uncertainty were underestimated; we can use a lower sampling frequency.

6. DISTANCE CALCULATIONS

In order to calculate distances to RR Lyrae stars, we needed to classify RR Lyrae subtypes as shown in Figure 4. However, there is currently only few systematic studies (calibrations) of the type classification using light curves only (mainly on types ab and c), and they are complicated in general. To avoid the

complications for the moment, we used the typical absolute RR Lyrae magnitude[10], $M_r \simeq M_V = 0.6$. To estimate the amount of dust reddening, we used the total to selective extinction[11], $R_V = 3.1$, and the number fraction weighted average color term[12], $(B-V)_0 = 0.358$, of RRab and RRc stars. The number fraction weighted average $(B-V)_0$ was calculated by using the number statistics of known RR Lyrae stars ($\simeq 91\%$ of RR Lyares are type ab and $\simeq 9\%$ of RR Lyraes are type c assuming that the numbers of Blazhko modulated and period doubling are negligible) as follows;

$$(B-V)_0 = 0.91(B-V)_{ab0} + 0.09(B-V)_{c0} \quad (4)$$

where $(B-V)_{ab0} \simeq 0.372$ and $(B-V)_{c0} \simeq 0.211$. Then the color extinction was calculated as[13];

$$E(B-V) = (B-V)_{observed} - (B-V)_0\,, \quad (5)$$

and the extinction was calculated as[13];

$$A_V = R_V E(B-V) \quad (6)$$

Finally, the distance was calculated by using the distance modulus;

$$d = 10^{[1+(m_r - A_V - M_V)/5]}\,. \quad (7)$$

To convert the gri magnitudes to the Johnson magnitudes, the conversions given by the Sloan Digital Sky Survey (SDSS)[14] were used. The error in the distance calculations were calculated by propagating errors assuming no covariance. The mean uncertainty in the distance was calculated to be $\simeq 20\%$, which disagrees with our SNR calculations for distance since we used the PL relation with a typical Z and did not take into account for the errors in the filter conversions and reddening. For better SNR calculations for distance, we need to consider better PL relations and the errors in the filter conversion and reddening.

7. RESULTS AND DISCUSSIONS

7.1. Spatial Distributions

From the calculated distances, the distance histogram of RR Lyrae stars is plotted and shown in Figure 5. It almost follows the Gaussian distribution, it might have been biased by the ATLAS Pathfinder telescope's sensitive magnitude range. The spatial distributions and histograms of RR Lyrae stars are shown in Figures 6 and 7, respectively. As in Figures 6a and 6c, we observed less number of RR Lyrae stars for the galactic latitude, $b < 0°$. This may be because the $b < 0°$ band are lower in both RA and Dec, so it was near the horizon, and we could not observe as well as the $b > 0°$ band. Or it could be purely because of the lower number density at $b < 0°$ than that at $b > 0°$. In order to fully determine the cause, we need to observe the same region by using observatories at more south latitudes. As in Figures 6b and 6d, the color extinction is more noticeable at $b < 0°$ than at $b > 0°$, which tells that there are more sources of reddening at $b < 0°$.

For the overall structure, we did not find clear spiral arm structures. As in Figures 7a and 7b, the galactic longitudinal distributions are patchy at both $b > 0°$ and $b < 0°$, but not conclusive enough. As in Figures 7c and 7d, the galactic latitudinal distributions are almost flat at both $b > 0°$ and $b < 0°$, which shows that the RR Lyrae stars are not concentrated on the galactic plane. Since RR Lyrae stars are old[5] ($\simeq 10$ Gyr), they have had a lot of time to drift. No clear spiral arm from the RR Lyrae spatial distribution tells that the galactic dynamics are complicated.

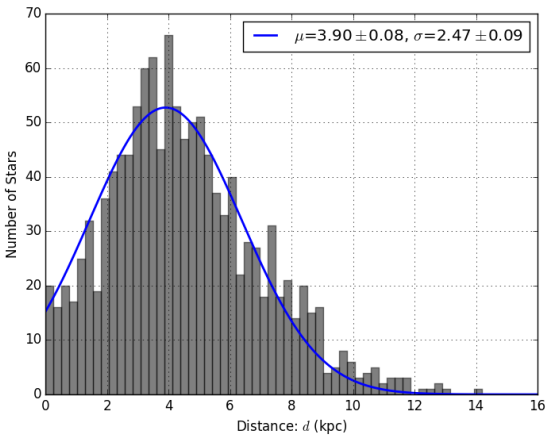

FIG. 5: *Distance histograms of 1,239 RR Lyrae stars with a Gaussian fit. The Gaussian fit was used to aid for seeing the general radial distribution of RR Lyrae stars.*

7.2. SIMBAD completeness

In order to evaluate the completeness of our results, comparisons needed to be made to other variable star catalogs. Simbad[15] provided a list of variable stars within our FOV. Pulsating sources encompasses all variable objects. With 48 objects overlapping our FOV, shown in Figure 8, we achieved a completeness of 98%.

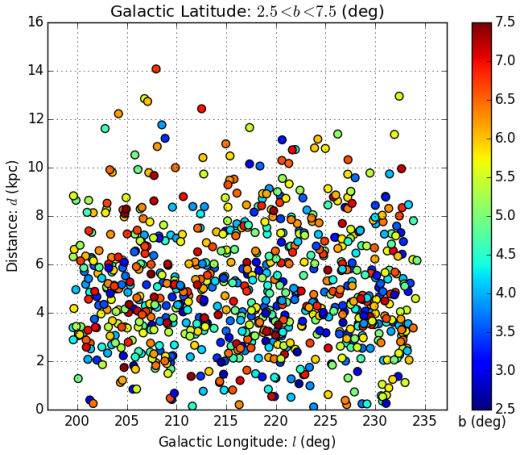

(a) $2.5 < b < 7.5$

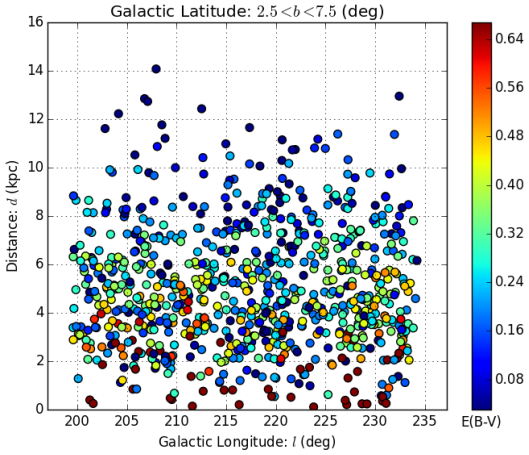

(b) $E(B-V)$ *for* $2.5 < b < 7.5$

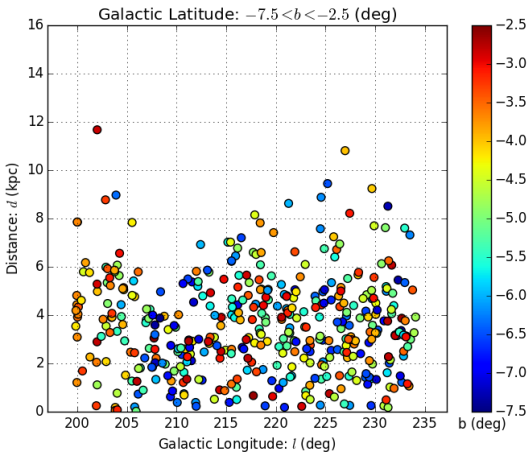

(c) $-7.5 < b < -2.5$

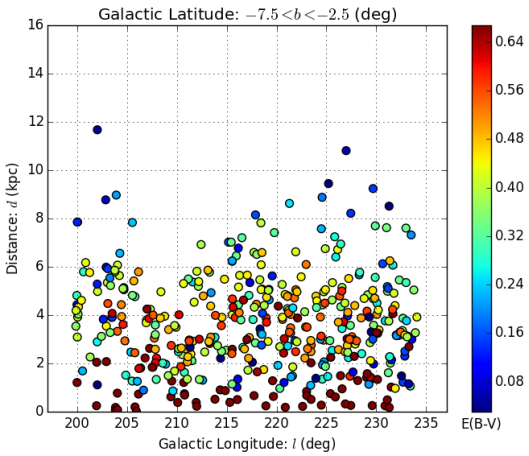

(d) $E(B-V)$ *for* $-7.5 < b < -2.5$

FIG. 6: *Spatial distributions of 1,239 RR Lyrae stars. The galactic longitude and latitude range correspond to our FOV. The range of* $E(B-V)$ *corresponds to the mean* $E(B-V) \pm 1\sigma$.

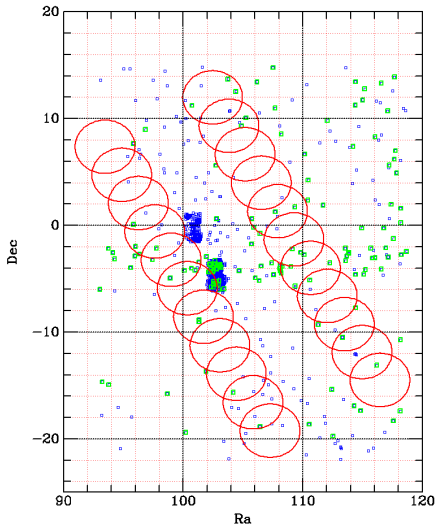

FIG. 8: *Observation path shown in red, with Simbad pulsators in blue and RR Lyrae in green.*

7.3. Evaluating the HPS Variability Parameter

A paper, *Finding, Characterizing and Classifying Variable Sources in Multi-Epoch Sky Surveys: QSOs and RR Lyrae in PS1 3π Data*[10] (HPS), quantifies the likelihood that a star is an RR Lyrae. Using their variability statistic, $\rho_{RRLyrae}$, density and distribution of RR Lyrae and other variable candidates were determined. Table I evaluates the validity of HPS's variability criteria.

Of the 1.5 Billion stars identified in our FOV, we isolated the 315,992 most variable, as described in § 2 2.3. A discussion on the determination of each objects variability classification is discussed in § 4. Data acquired from external variable star catalogs was immediately restricted by magnitude and FOV. To most accurately restrict obtained data, given RA and Dec values were converted to galactic coordi-

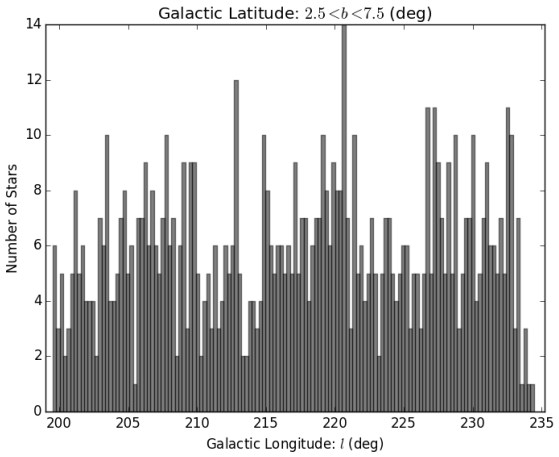

(a) *Galactic longitudinal histogram for* $2.5 < b < 7.5$

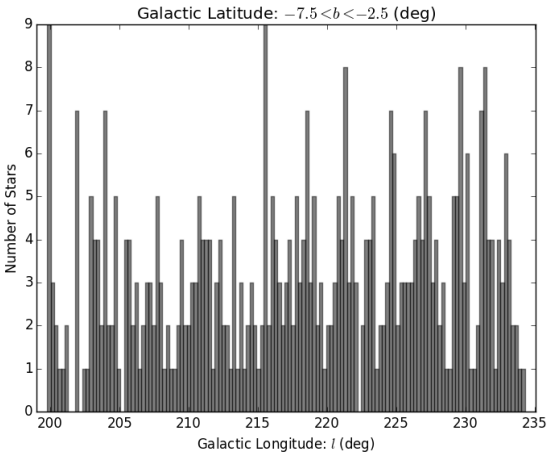

(b) *Galactic longitudinal histogram for* $-7.5 < b < -2.5$

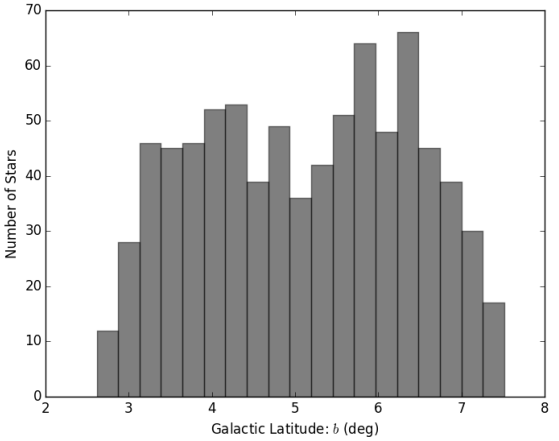

(c) *Galactic latitudinal histogram for* $2.5 < b < 7.5$

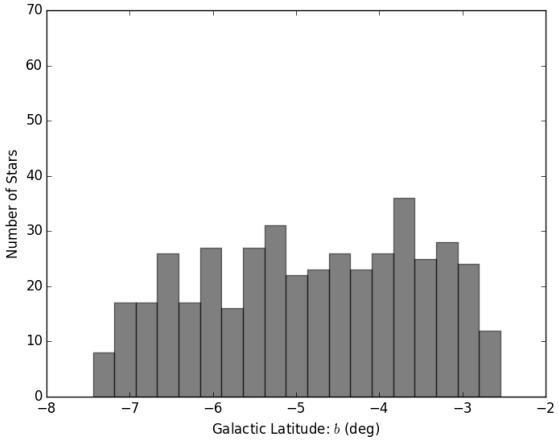

(d) *Galactic latitudinal histogram for* $-7.5 < b < -2.5$

FIG. 7: *Spatial histograms of 1,239 RR Lyrae stars. The galactic longitude and latitude range correspond to our FOV.*

nates. Once converted, stars residing in our observed FOV were isolated for comparison. Due to detection limits of our instruments, the mean magnitude in each bandpass was restricted ($m_g \leq 16$, $m_r \leq 16$, $m_i \leq 16$). Outlined in Table I are the results of comparing observations with HPS data. HPS_{total} is the total number of HPS stars in our FOV, $HPS_{matched}$ is the number of objects matched to observed stars, $HPS_{completeness}$ describes the fraction of HPS data that matched to our observations. The columns $RRLyrae$ and $NotRRLyrae$ describe the number of observed and verified stars that matched to HPS data. To calculate $Prob(RR)$ and $Prob(notRR)$, the number of observed stars was divided by the number of HPS stars, for each $\rho_{RRLyrae}$ range.

A grouping and matching algorithm, written by J. Tonry[1], made it possible to isolate and group stars from various nights of observations. Implementation of logPr(rnd) allowed for complete confirmation of RR Lyrae candidates. Only stars with different variable classifications, those having lower amplitude variations, would have been able to go undetected. Masking out regions of high aliasing reduced the need to run a more rigorous analysis, due to the statistically improbability of these sources being variable. A total of 5,658 stars fell within the masked region, shown in Figure **??**. FLS and FSS analysis identified 1,239 variable stars in our FOV. A defining characteristic of RR Lyrae is their variability periods, falling between 0.05 and 1.2 days. Using this restriction, 244 confirmed to be RR Lyrae matched the HPS dataset. Variability classification was confirmed by visually inspecting the light curves of all 244 RR Lyrae candidates as well as the remaining 995 unclassified variable stars. Following this procedure gives us 100% purity.

HPS $\rho_{RRLyrae}$	HPS_{total}	$HPS_{matched}$	$HPS_{completeness}$	RR Lyrae	Not RR Lyrae	Prob(RR)	Prob(notRR)
0.0-0.05	5029	138	0.27	46	92	0.33	0.67
0.05-0.1	124	25	0.20	12	13	0.48	0.52
0.1-0.2	154	38	0.25	19	19	0.50	0.50
0.2-0.3	116	36	0.31	15	21	0.42	0.58
0.3-0.4	82	36	0.44	22	14	0.61	0.39
0.4-0.5	85	34	0.40	20	14	0.59	0.41
0.5-0.6	90	41	0.46	22	19	0.54	0.46
0.6-0.7	89	47	0.53	28	19	0.60	0.40
0.7-0.8	64	39	0.61	28	11	0.72	0.28
0.8-0.9	46	28	0.61	23	5	0.82	0.18
0.9-1.0	21	15	0.71	9	6	0.60	0.40
0.0-1.0	5900	477	0.08	244	233	0.51	0.49

TABLE I: A comparison of verified observations and HPS RR Lyrae candidates. In this table, data is separated into various ranges of HPS's RR Lyrae variability criteria, $\rho_{RRLyrae}$. Integer values represent the number of stars that lie within a particular range. The three values given as decimals ($HPS_{completeness}$, Prob(RR), and Prob(notRR)) represent fractional percentages. Calculation methods of each column is discussed in § 7 7.3.

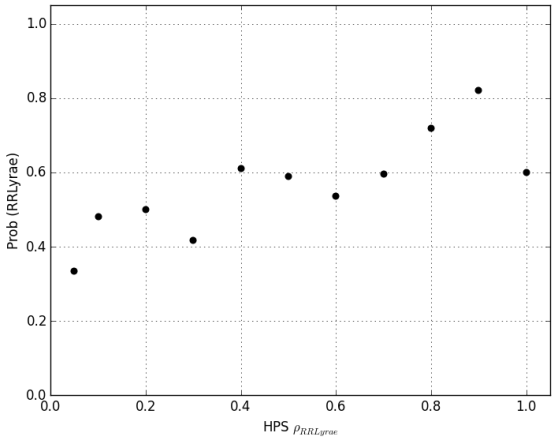

FIG. 9: *Evaluation of HPS RR Lyrae criteria, using matched RR Lyrae.*

The same matching algorithm[1] made comparing observations with other variable catalogs possible. To evaluate the HPS RR Lyrae criteria, our observations were matched to stars analyzed for variability, by HPS. Shown in Table I and Figure 9, there is no correlation between HPS criteria and verified RR Lyrae stars. HPS claims any star with an assigned $\rho_{RRLyrae} \geq 0.20$, is most likely an RR Lyrae. Furthermore, if $\rho_{RRLyrae} \geq 0.05$, the candidate is definitively an RR Lyrae. Figure 9 shows the fractional portion of observed RR Lyrae, that matched to stars that have been assigned $\rho_{RRLyrae}$, by HPS. There is a distinct correlation between confirmed RR Lyrae and assigned $\rho_{RRLyrae}$ values. However, over 16% of all observed RR Lyrae, that matched to HPS stars, have $\rho_{RRLyrae} \leq 0.20$. Similarly, 10% of all matched RR Lyrae fall below $\rho_{RRLyrae} \leq 0.05$. Of all 244 matched RR Lyrae, only 9 have the highest RR Lyrae probability assigned, $\rho_{RRLyrae} \geq 0.90$.

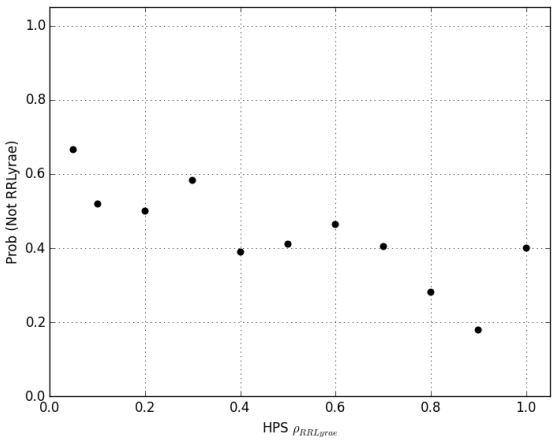

FIG. 10: *Evaluation of HPS RR Lyrae criteria, using stars that have been matched and verified not to be RR Lyrae.*

Shown in Figure 10, there exists an inverse relationship, between non-RR Lyrae confirmed stars and HPS assigned $\rho_{RRLyrae}$. All stars confirmed as not begin RR Lyrae should have assigned $\rho_{RRLyrae} \geq 0.20$, according to HPS; yet 23% of all matched stars do not meet this criteria. Complete validity of HPS's $\rho_{RRLyrae}$ would be indicated by 0 verified, non-RR Lyrae, stars being matched with a $\rho_{RRLyrae} \geq 0.05$. This is not the case, with 30% of all matched stars begin confirmed non-RR Lyrae and having an assigned $\rho_{RRLyrae} \geq 0.05$. While HPS's

$\rho_{RRLyrae}$ may indicate if a star is an RR Lyrae, it is not sufficient for absolute determination.

8. CONCLUSIONS AND FUTURE OPPORTUNITIES

We used the ATLAS Pathfinder telescope to survey RR Lyrae stars. This allowed us to study the galactic structure and evaluate the HPS variability parameters, over our approximately 340 deg^2 FOV. Due to the low angular resolution of the ATLAS Pathfinder Telescope, as well as the observable sky at the time of our observations, we chose our FOV to be $202^\circ \leq l \leq 232^\circ$ centered at $b = \pm 5^\circ$, slightly above and below the galactic plane. Our observations spanned 20 nights with 10 observations per night, in each filter, to achieve the desired period accuracy of $\simeq 1\%$. An exposure time of 20 sec was used to achieve $\simeq 10\%$ photometry. We obtained roughly 1.5 billion light curves and applied the quartile criteria, FLS, and FSS to identify 1,239 RR Lyrae variables, with mean period uncertainty of 0.15%.

To avoid complicated type classifications using only light curves, the mean RR Lyrae magnitude of $M_r \simeq M_V = 0.6$ was used in calculating distances. The dust extinction was estimated by adopting the total to selective extinction, $R_V = 3.1$, and the mean RR Lyrae color term, $(B-V)_0 = 0.358$. The mean uncertainty in calculated distances was roughly 20%. Using calculated distances, the spatial distribution of RR Lyrae stars was analyzed. Our observations showed fewer RR Lyrae stars at values of $b < 0^\circ$. A possible explanation for this is that our field was closer to the horizon. We found higher dust extinction values at $b < 0^\circ$; suggesting the existence of more reddening sources, at lower galactic latitudes. The longitudinal distributions were shown to be patchy, with flat latitudinal distributions; showing no clear spiral arm structures. Apparently random spatial distribution of RR Lyraes, coupled with their old ages, suggests quite complicated galactic dynamics.

Pan-STARRS objects were evaluated by HPS. Each stellar candidate was assigned a $\rho_{RRLyrae}$ value, signifying the likelihood of it being a RR Lyrae. With only a weak correlation shown

Now that we found more than 1,000 RR Lyrae stars in our FOV, we can use these to construct statistics for RR Lyrae subtype classifications purely from their light curves (not only types ab and c, but also ones with the Blazhko effects). In order to do that, we need spectra of the RR Lyrae stars to calibrate the statistics. If there are any significant correlations between RR Lyrae light curve shapes and physical properties, then we can used the statistics to measure the physical properties of RR Lyrae stars from thier light curves.

ACKNOWLEDGMENTS

We would like to thank John Tonry, Conor McPartland, Marielle Dela Cruz, and Jeff Kleyner.

* dhiramat@hawaii.edu
† cmutnik@hawaii.edu

[1] J. L. Tonry, personal communication (2016).
[2] *Asteroid terrestrial-impact last alert system*, http://fallingstar.com/specifications.php (2016).
[3] L. Molnár, R. Szabó, P. A. Moskalik, J. M. Nemec, E. Guggenberger, R. Smolec, R. Poleski, E. Plachy, K. Kolenberg, and Z. Kolláth, **452**, 4283 (2015), 1507.04714.
[4] C. Cáceres and M. Catelan, **179**, 242-248 (2008), 0805.3704.
[5] B. S. Rayden and B. M. Peterson, *Foundations of Astrophysics* (San Francisco: Addison-Wesley, 2010), 1st ed.
[6] *American association of varaible star observars*, https://www.aavso.org/types-variables (2012).
[7] W. H. Press and G. B. Rybicki, Astrophys. J. **338**, 277 (1989).
[8] W. H. Press, S. A. Teukolsky, W. T. Vetterling, and B. P. Flannery, *NUMERICAL RECIPES* (Cambridge: Cambridge University Press, 2007), 3rd ed.
[9] J. T. VanderPlas and Ž. Iveacute, **812**, 18 (2015), 1502.01344.
[10] N. Hernitschek, E. F. Schlafly, B. Sesar, H.-W. Rix, D. W. Hogg, Ž. Ivezić, E. K. Grebel, E. F. Bell, N. F. Martin, W. S. Burgett, et al., Astrophys. J. **817**, 73 (2016), 1511.05527.
[11] E. L. Fitzpatrick, Publications of the Astronomical Society of the Pacific **111**, 63 (1999), URL `http://stacks.iop.org/1538-3873/111/i=755/a=63`.
[12] J. M. Nemec, **127**, 2185 (2004).
[13] B. W. Carroll and D. A. Ostlie, *An Introduction to Modern Astrophysics* (San Francisco: Addison-Wesley, 2007), 2nd ed.
[14] M. Fukugita, T. Ichikawa, J. E. Gunn, M. Doi, K. Shimasaku, and D. P. Schneider, Astron. J. **111**, 1748 (1996).
[15] M. Wenger, F. Ochsenbein, D. Egret, P. Dubois, F. Bonnarel, S. Borde, F. Genova, G. Jasniewicz, S. Laloë, S. Lesteven, et al., aaps **143**, 9 (2000), astro-ph/0002110.